The Khione Bag

Kade Jimenez, Adriana Delagarza, Kate Lampo, and Kalen Richardson

The authors are with the Department of Mechanical Engineering, Columbia University, New York, NY (kaden.j@columbia.edu, ad3921@columbia.edu, k.lampo@columbia.edu, kfr2115@columbia.edu. This material is based upon work developed in the MECE E3420 / E3430 Engineering Design Courses.

***Abstract*— A novel avalanche airbag design is proposed to address the technical limitations of current products and to increase the accessibility of avalanche safety gear. The Khione bag uses a dual-walled deployment scheme, can passively deliver oxygen to recreationists in peril, and a implements novel sleeved form factor. It is also backpack-agnostic, meshing with a user's existing gear instead of requiring the purchase of an expensive integrated setup.**

The dual-walled inflation mechanism is explored in simulation and via a reduced prototype. Simulation validates a faster inflation time for the dual-walled scheme, as does low-pressure testing of the physical prototype.

The strength of the airbag material—TPU-coated ripstop nylon—is also explored. The durability of heat-sealed seams, the airbag's ruggedness when cyclically loaded, and the material strength at operation temperatures are all tested for several types of prototype fabric. Results confirm that a lightweight ripstop nylon is sufficient to meet published loading standards for avalanche airbags.

I. Introduction

Every year, there are around 100,000 avalanches in the Western United States, with around 150 avalanche-related deaths across the globe [1], [2]. Avalanche mortality is largely caused by asphyxiation, which occurs when recreationists get trapped beneath heavy snow with no access to breathing air.

When the snow in an avalanche begins to move, it acts like a pseudo-fluid, catching anyone and anything in its path. Avalanche airbags capitalize on this flowing snow in order to provide individual users with buoyancy when they are caught in an avalanche event. This personal protection equipment helps keep victims as close to the surface as possible, increasing their odds of survival by decreasing their burial depth [3].

There are a number of existing avalanche airbags on the market, but they are limited in their capacity as full personal protection equipment. More specifically, they are only designed to provide buoyancy during an avalanche event. Other non-buoyancy avalanche safety gear has focused on access to air under the snowpack in the event of burial, but that technology has yet to be integrated into an airbag [3]. (Though, there has been some limited recent research on actively deflating an avalanche airbag post-burial in order to make an air pocket that can be used to expand a user's air supply [4].)

Another drawback of the avalanche airbags on the market is their lack of modularity. Current designs come preinstalled into a backpack with a large price tag attached. Thus, we see an opportunity to borrow from preexisting avalanche airbag and personal protection technology (as well as recent research in this area) in order to make a high-performance airbag.

To address this need for more accessible protection against avalanches, we have redesigned the traditional avalanche airbag. The Khione bag incorporates a dual-walled inflation structure for faster deployment, passive air delivery for a longer-lasting oxygen supply, and a protective, over-the-shoulder form factor. The airbag is also backpack-agnostic, meshing with a user's existing gear instead of requiring the purchase of an expensive integrated setup.

The British Standards Institution formed the basis for most of our design constraints, as building an airbag that can be operated safely and reliably by a user is our top priority. EN16716 advises that avalanche airbags be at least 150 liters in volume, able to operate in temperatures of at least -30°C, and fully inflate in fewer than five seconds, amongst other requirements [5]. In this paper, we explore standards related to inflation and durability as directly applicable to the Khione Bag.

II. Dual-Walled Inflation: Fluids Analysis

A. Methods

Given that the the buoyancy generated by the airbag is proportional to the volume, it is critical that the bag inflate as quickly as possible to minimize the chances that a user gets buried during the inflation process. In addition, standard EN16716 mandates complete inflation in less than 5 seconds. In order to inflate rapidly, the Khione bag implements a dual-walled inflation scheme. The scheme separates the airbag into two nested chambers, a cross section of which is depicted in Figure 1.

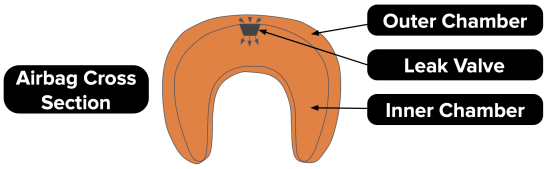

Fig. 1. Sketch of the vertical cross-section of a dual-walled airbag.

Air first flows from a compressed cylinder into the outer chamber, inflating the bag as a shell and ensuring that maximum displacement volume is reached quickly. At the same time, a large one-way valve attached to the inner airbag allows ambient air in to prevent the formation of a vacuum. Between the inner and outer airbag chambers, a leak valve then allows air to flow from the shell to the inner chamber, forcing pressure to homogenize over time to minimize overall airbag compressibility. The size of the leak valve in this case becomes a critical design factor; if it is too large, the airbag will function as if it had a single chamber design, and if it too small, the pressure in the outer chamber could put unwanted stress on the fabric.

In order to validate the assumption that the inflation scheme would function as planned, the system was modeled using two computational models and a simplified physical prototype.

1) Inflation Model Assumptions: The goal of the computational model was to derive a set of ODEs that theoretically proved that dual-walled inflation would result in more rapid initial inflation. Modeling the deformation of the volume depended upon an extremely wide number of variables, so to make the system solvable, pressure was used as a proxy for inflation. The force required to deform the bag from its deflated to inflated state was assumed to be negligible relative to the force applied on the airbag as a result of the

pressure differential. This in turn allowed the assumption that the airbag chambers could be considered to be rigid volumes that started at 0 gauge pressure. The simplified system can be seen in Figure 2.

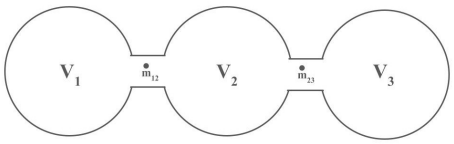

Fig. 2. Simplified concept sketch of the dual-walled inflation system.

Here, V_1 represents the air cylinder volume, V_2 represents the outer airbag chamber volume, V_3 represents the inner airbag chamber volume, $\dot{m}_{12}$ represents the mass flow rate between the air cylinder and the outer chamber, and $\dot{m}_{23}$ represents the mass flow rate between the outer chamber and the inner chamber. Note that the naming scheme will follow the same trend for all state variables: T_1 represents the temperature in the air cylinder, p_2 represents the pressure in the outer chamber, etc.

Although exact volume deformation is unknown in this scheme, general inflation trends can be observed by analyzing the relative pressure in each chamber.

2) Adiabatic Case: In order to set up our system of ODEs to represent this simplified system, we further assumed that all processes were considered one-dimensional and isentropic. One-dimensionality was assumed for simplicity and is a potential source of small error. The isentropic assumption was made with the understanding that the speed of the process is fast enough that heat exchange with the surroundings is negligible [6]. Ideal gas behavior was assumed, which may have been an inappropriate assumption given the high pressure of the air cylinder used to inflate the airbag, and will be discussed further when noting the results of the computational model. This gave us a set of ideal gas equations that could approximate the air flow behavior. The first equation is the ideal gas law in the form: $pV = mRT$ where P is pressure, V is volume, m is the mass of the gas, R is the specific gas constant of air, and T is the temperature of the gas [6]. Solving for p and T and differentiating with respect to time, we get:

$$\frac{dp}{dt} = \frac{R}{V}\left(\dot{m}T + m\frac{dT}{dt}\right) \tag{1}$$

where $\dot{m}$ is the mass flow rate $-\frac{dm}{dt}$. $\dot{m}$ can be solved for directly by using the equations for mass flow rate of an ideal compressible gas in a choked channel:

$$\dot{m} = C_d A p_0 \sqrt{\frac{2\gamma}{RT_0(\gamma-1)}\left[\left(\frac{p}{p_0}\right)^{\frac{2}{\gamma}} - \left(\frac{p}{p_0}\right)^{\frac{\gamma-1}{\gamma}}\right]} \tag{2}$$

where A is the area at the narrowest point in the channel, p_0 is the upstream pressure, p is the downstream pressure, T_0 is the upstream temperature, γ is the ratio of specific heat capacities for air (C_p/C_v), and C_d is the discharge coefficient [7] [8]. Mass flow reaches a maximum when the flow becomes sonic, and the equation simplifies to:

$$\dot{m}_{choked} = C_d A p_0 \sqrt{\frac{\gamma}{RT}}\left(\frac{2}{\gamma+1}\right)^{-\frac{\gamma+1}{2(\gamma-1)}} \tag{3}$$

Given the ideal gas assumption, it is reasonable to also assume that the specific heat of air is constant, allowing for the solution of an equation for $\frac{dT}{dt}$. This is achieved by using the second law of thermodynamics for an isentropic process in the form:

$$Tp^{\frac{\gamma-1}{\gamma}} = const. \tag{4}$$

Taking the time derivative and solving for $\frac{dT}{dt}$,

$$\frac{dT}{dt} = \frac{T}{p}\left(\frac{\gamma-1}{\gamma}\right)\frac{dp}{dt} \tag{5}$$

By consolidating equations 1, 2, 3, and 5, the system can be simplified into a series of coupled ODEs. Through implementation in the SciPy Python library, the equations can be solved for a set of initial conditions using a Runge-Kutta method. The full set of initial conditions and constants are outlined in the Appendix. The code uses the RK45 algorithm to solve the 2 coupled ODEs (equations 1 and 5), with one Python function to calculate $\dot{m}$ (conditionally using equations 2 and 3). These conditions were simulated for 15 seconds for three different nozzle sizes: 0.1, 0.5, and 1.0 inch diameter circles.

3) Isothermal Case: In a secondary inflation analysis, an isothermal case is investigated. This assumption is to some degree inaccurate, as the rapid depressurization of the compressed air cylinder will result in temperature shifts. However, the isothermal case is useful as the high initial pressure in the compressed air cylinder results in nonphysical temperatures (discussed further in the results section). By comparing the temperature-varying and isothermal cases, overall trends can be noted that account for inaccuracies that arise from inappropriate assumptions.

All of the equations discussed above apply to the isothermal case and are simply modified with the consideration that $\frac{dT}{dt} = 0$, so equation 5 is no longer relevant. Three simulations were run with identical nozzle sizes as those used in the adiabatic case.

4) Physical Validation: In order to physically validate the simulations, a simplified physical model of the airbag was manufactured. A sketch of the model can be seen in Figure 3, and the manufactured model can be seen in Figure 4.

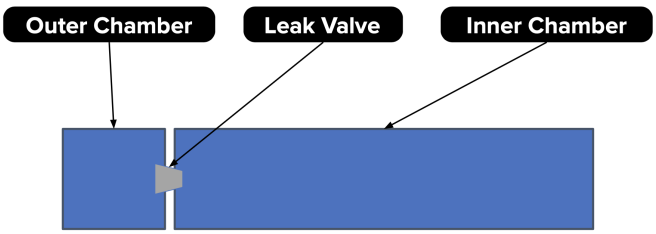

Fig. 3. Sketch of simplified physical fluids model.

The two chambers, while scaled down, keep the same volume ratio as the actual airbag. The nozzle area was

Fig. 4. Fully-inflated simplified fluids model.

selected based off of the results of the simulations discussed below. In order to fully inflate the chambers, a constant input from a high pressure line of roughly 125 psi was applied. This analysis was fully qualitative, with inflation recorded and analyzed to see the times at which each chamber reached its maximum volume.

B. Results

1) Computational Models: Results for the two computational models are are given in Figs. 5, 7, 8, and 9.

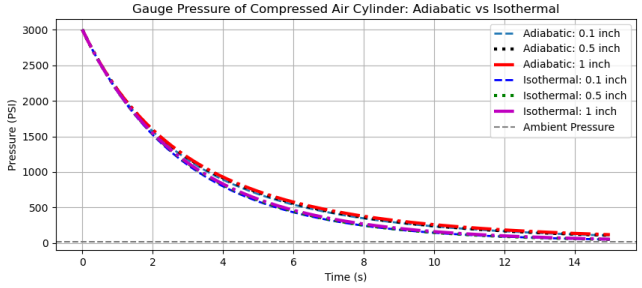

Fig. 5. Cylinder pressure across both adiabatic and isothermal simulations.

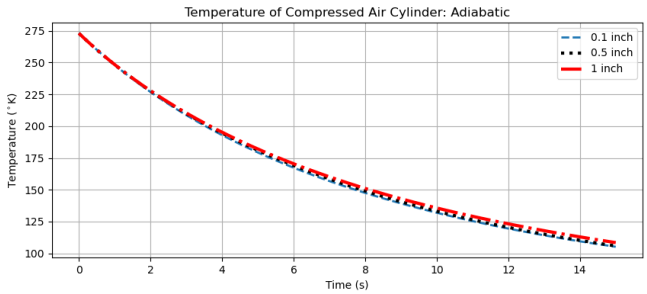

Fig. 6. Cylinder temperature across adiabatic simulations.

2) Physical Validation: A diagram and image of the inflation of the simplified physical prototype can be seen in Figs. 3 and 4, respectively. The diameter of the nozzle was selected to be $3/4$" based off of computational simulations. When the continuous 125 psi stream of air was provided, the first chamber reached its maximum volume in approximately 3 seconds, while the second reached complete inflation in roughly 15 seconds (Fig. 4).

C. Discussion

1) Adiabatic Simulation: Looking at the adiabatic simulations, the first trend that can be qualitatively noted is the lack of change in the dispersion rate of the air cylinder between all trials. The pressure of the cylinder is plotted against time in Fig. 5, where there is negligible variation between trials. The consistency indicates that no matter which set of assumptions is made, a small nozzle between the two airbag

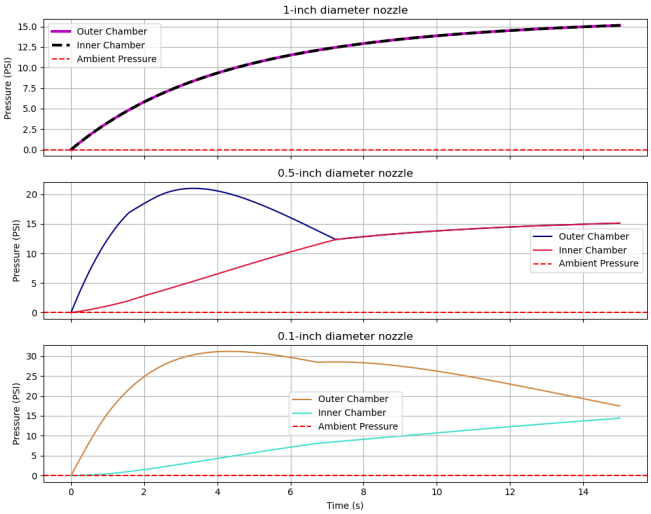

Fig. 7. Airbag chamber pressures over time for the adiabatic simulation.

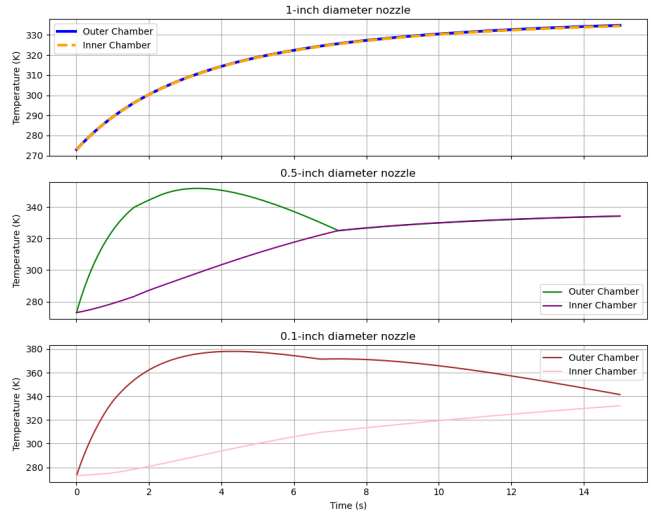

Fig. 8. Airbag chamber temperatures over time for the adiabatic simulations.

chambers won't impede the overall inflation. This indicates that controlling the nozzle size shouldn't increase inflation time; rather, it will affect the distribution of the air between the chambers over time.

This behavior is further supported by Fig. 7. The sizing of the nozzle results in varying pressure differentials between the two airbag chambers. Despite the different initial behavior, in all cases the entire airbag eventually approaches a homogeneous pressure of roughly 15 psi.

Another important trend to address is the unrealistic temperature predictions during airbag inflation. As shown in Figures 8 and 6, the simulated temperature of air coming out of the cylinder stabilizes around 100°K and air temperatures in the airbag chambers stabilize °K between 300 and 350 °K. These values that are implausible given the system's enthalpy. In rapid inflation scenarios, the stagnation enthalpy of the gas should remain approximately constant [9]. Stagnation enthalpy is defined as $h_0 = h + v^2 = C_p T + \frac{v^2}{2}$, where h is the static enthalpy and v is the velocity of the fluid. Assuming minimal loss in h_0, once the gas comes to rest

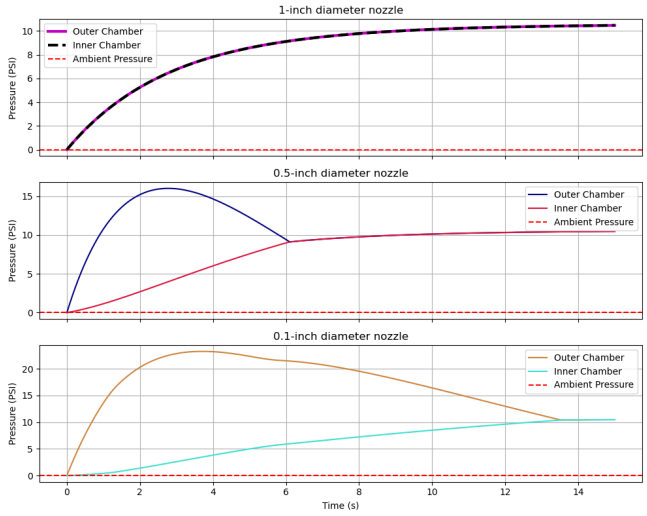

Fig. 9. Airbag chamber pressures over time for the isothermal simulation.

(v=0), the change in static enthalpy (and thus temperature) should be relatively small.

Given the rapid nature of deployment, the assumption of negligible change in stagnation enthalpy implies the post-inflation air temperature should be relatively uniform. While assuming isothermal conditions may not be entirely realistic, it offers a conservative approximation that can be used as a point of comparison for the adiabatic case. As such, the isothermal and adiabatic models can be interpreted as bounding cases, with the actual final pressure likely falling between their predictions.

2) Isothermal Simulation: The first thing that can be noted from the results of the isothermal simulation is the similarity in overall trends to the adiabatic simulation. As was seen in adiabatic tests, with decreasing nozzle size comes a larger pressure differential. The lack of fluctuation in temperature results in the air reaching a more stable, lower equilibrium pressure slightly above 11 psi. This number allows to predict that the actual equilibrium pressure will lie between 11 and 15 psi.

All of the above results indicate that a properly-sized valve should give us the desired inflation scheme to allow the dual-walled inflation to function as intended. Recalling that pressure is being used analogously with volume, the pressure differential achieved between the two airbag chambers seen in Figs. 7 and 9 should result in the overall airbag inflating initially as a shell before pressure homogenizes to minimize compressibility. With decreasing nozzle area, the pressure differential becomes more severe, reducing the time required to hit the maximum volume of the airbag. However, with increasing pressure differential comes higher stresses applied on the airbag and a longer time until an equilibrium pressure is reached, leaving the bag more susceptible to deformation from the compressive force of the snow.

Taking all of the above into account, a nozzle diameter of $3/4$" was selected for the final design, as it is the smallest diameter nozzle that reached homogeneous pressure between chambers within 5 seconds, thus meeting EN16716 [5].

3) Physical Validation: The simplified physical model further adds evidence that the simulation values are reasonably good predictors of behavior. Critically, after selecting a nozzle size informed by the simulation results, the inflation model functioned as predicted, which is to say that the initial chamber reached its maximum volume notably faster than the second chamber. While the specific times are not good indicators of a full prototype's inflation time, the general trends are worth noting, given that the prototype is a scaled down model with a simplified geometry. The results indicate that at a qualitative level, the nozzle size is reasonable, and in a full prototype, the inflation scheme should function as predicted.

III. Breaking Pressure: Tensile Testing

In addition to exploring dual-walled inflation, we also conducted a series of tensile tests to study the mechanical properties of the TPU-coated ripstop fabric that makes up the majority of our design.

A. Methods

Guided by EN16716, we ran four different types of tests: material strength, seam strength, cyclic loading, and temperature-variable strength [5]. We also chose to use three different TPU-coated ripstop materials, each representing one of our airbag prototypes: single-sided coating [SS], double-sided thick coating [DSK], and double-sided thin coating [DSN]. In total, we conducted tests for every permutation of material paired with test type. The one exception to this was the temperature tests of the thin double-sided fabric, which we were unable to conduct due to material procurement constraints. For each combination, we performed three different trials.

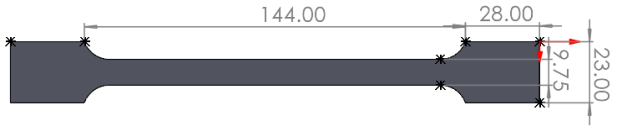

Fig. 10. Dimensioned drawing of dogbone shape [mm]

1) Material and Seam Strength Testing: Material strength testing involved tracing three dogbone shapes (Fig. 10) onto each type of material, cutting samples with fabric scissors, and clamping the material in an Instron Universal Testing Machine's grips. Note here that no extra material was placed between the tensile grips and the dogbones to prevent the airbag material from slipping; instead, we relied heavily on the geometry of the dogbones to allow the material to tear before it could slide against the grips.

Seam strength testing began by tracing pairs of 2-inch-by-7-inch strips of each material type, cutting samples with fabric scissors, placing one strip directly atop another, and sealing the two on an inch-long section at the top of the strips. To seal, a leather iron was pressed sideways against the pieces of fabric such that the entire width of the iron laid on the material. After ten seconds of pressure had been applied,

the iron was removed and a roller was used for ten seconds to secure the seal. This process of heating and rolling was repeated once more. A similar method was used for actual airbag fabrication, making the seam creation representative of the design.

For material strength and seam strength tests, we utilized a built-in Instron tensile test with pre-loading. SS and DSK samples were manually pre-loaded to 20N, and DSN samples were pre-loaded to 10N. The DSN samples were thinner, so a lower pre-load value was thought to be more appropriate. Once manually pre-loaded, the displacement was zeroed, and the test was started. Both material strength and seam strength tests pulled the sample at a constant rate of 0.2 mm/s. Pre-load values were later accounted for in data processing to ensure consistent results.

2) Cyclic Testing: For cyclical loading tests, samples were loaded into the grips and tightened in a similar fashion. However, a custom Instron method was used. The test started with an automatic pretension step of 10N followed by a hold for two seconds and loading up to 40N at a rate of 1mm/s. After the sample was loaded to 40N, it was allowed to relax, ramping down to 5mm below its initial displacement and allowing for a re-zeroing of the force sensor. This re-zeroing is an important step, as the force sensor has a tendency to drift when loaded. The hold step was implemented after the preloading step so that there was enough data to pull the cycle "starting" displacement. This value was used during analysis, since the software did not allow for re-zeroing of displacement.

The samples underwent 20 loading cycles. This is consistent with the cyclical loading standard that avalanche airbags must meet; they must be able to inflate 20 times without catastrophic damage to the airbag material [5].

3) Temperature Testing: Finally, for temperature tests, three dogbones were cut out of the DSK material and three dogbones were cut out of the SS material. All six samples were placed into a -20°C freezer for 24 hours, then removed one at a time and tested. However, there were unfortunately many limitations to this experimental setup. Firstly, the freezer we had access to was located inside a laboratory on the medical campus, and since it was crucial that we test our fabric directly after removing it from the freezer, we also ended up having to test the strength of our fabric using an Instron in that same lab. The Instron used was set up to test short pieces of cervical tissue, and in order to minimize disruptions to this setup, it was advised that shorter pieces of our material were tested as opposed to the full dogbones.

Ultimately, we chose to test pieces of fabric that were approximately 1 inch in length and 0.5 inches in width. A 1 kN load cell was used to pull all fabric at a rate of around 1.3 mm/s for a standard tensile setup. To discourage the fabric from slipping between the tensile grips, sandpaper was superglued to the inner faces of the grips and they were tightened firmly.

4) Data Analysis: After collecting force and displacement data for each trial, we computed the stress, σ, and the strain, ϵ, as such:

$$\sigma = F/A; \quad \epsilon = \frac{l - l_0}{l_0} * 100 \tag{6}$$

Here, F is the force, A is the cross-sectional area of the sample, l is displacement length, and l_0 is initial length.

We then proceeded with analysis for the material, seam, and temperature tests, all of which were conducted to failure. To do so, we plotted stress versus strain for each sample, giving us a visual depiction of each trial. Because we were working with brittle materials, the variables exhibited a linear relationship, indicating that the samples underwent only elastic deformation, not plastic deformation. In context, this makes sense: the most reasonable failure mode of the Khione bag is bursting, not permanent deformation or stretching. To confirm this hypothesis, we fit a linear curve to each sample, computing R^2 values to validate linearity. For our purposes, we required R^2 values of 0.95 or above to proceed [5].

Having confirmed linearity, we then computed the ultimate tensile strength σ_u of each sample by identifying the maximum stress each experienced. (Because we assume our samples deform entirely elastically, this is also the fracture point.) Finally, we compared the performance of each sample to the relevant standards, allowing us to draw conclusions about the safety of our design.

To seperately analyze the cyclic tests, we decided to evaluate the change in deformation over time to determine whether or not there was a significant change in strain when repeatedly applying the same force to the airbag. To accomplish this, we plotted strain versus time for the entire set of cycles and identified the local maxima (ie. the maximum strain for each cycle). We then computed the simple difference in maximum strain between the first and last cycles to compare.

B. Results

A sample plot for one trial with its accompanying linear fit is given in Fig. 11. For clarity and readability, every fifth data point is plotted, rather than each individual sample.

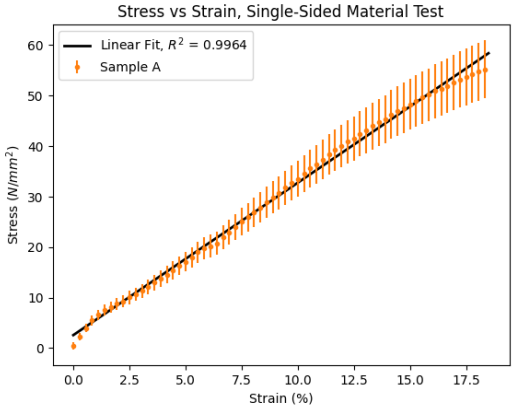

Fig. 11. Sample stress vs strain plot with a linear fit.

The computed R^2 values for each fit are given in Table I.

Next, the averaged σ_u values for each test (calculated using the applicable trials based on their R^2 values) are given

Material	Trial	Test Type		
		Material	Seam	Temperature
SS	A	0.996	0.707	0.116
	B	0.996	0.994	0.993
	C	0.994	0.988	0.999
DSK	A	0.994	0.996	0.979
	B	0.994	0.999	0.961
	C	0.993	0.999	0.958
DSN	A	0.992	0.021	n/a
	B	0.995	0.144	n/a
	C	0.995	0.025	n/a

TABLE I

R-SQUARED VALUES FOR EACH TEST.

in Table II. Derivation of uncertainty propagation is given in the Appendix.

Material	Trial	Test Type		
		Material	Seam	Temperature
SS	A	56 ± 6	n/a	n/a
	B	56 ± 6	67 ± 7	210 ± 22
	C	62 ± 6	46 ± 5	185 ± 19
	AVG	58 ± 3	57 ± 4	197 ± 14
DSK	A	33 ± 4	33 ± 4	37 ± 3
	B	36 ± 4	28 ± 3	50 ± 5
	C	36 ± 4	42 ± 4	39 ± 4
	AVG	35 ± 2	32 ± 2	42 ± 2
DSN	A	26 ± 3	n/a	n/a
	B	27 ± 3	n/a	n/a
	C	31 ± 3	n/a	n/a
	AVG	28 ± 2	n/a	n/a

TABLE II

ULTIMATE TENSILE STRENGTH VALUES FOR EACH APPLICABLE TEST.

Finally, Table III provides the difference in strain between the first and last trial of each cyclic test.

Material	Trial	Strain Difference
SS	A	0.69 ± 0.8
	B	1.08 ± 0.08
	C	0.76 ± 0.06
	AVG	0.85 ± 0.04
DSK	A	0.9 ± 0.1
	B	1.8 ± 0.2
	C	1.4 ± 0.3
	AVG	2.6 ± 0.2
DSN	A	n/a
	B	3.1 ± 0.2
	C	2.3 ± 0.2
	AVG	1.4 ± 0.1

TABLE III

VARIATION IN ULTIMATE TENSILE STRENGTH VALUES BETWEEN THE FIRST AND LAST CYCLE IN EACH CYCLIC TEST.

C. Discussion

Overall, our results demonstrate that our manufacturing methods meet avalanche airbag standards, and that the TPU-coated ripstop fabric we have chosen to use is sufficient for our application. Engineering Standard EN 16716 mandates that the airbag must be able to withstand a pressure of 0.1 N/mm^2, and our materials all outperform that by several orders of magnitude [5].

Beginning with the material tests, we see that all nine trials across all three materials met a strict linearity condition, supporting our hypothesis that the material fails elastically. Also as expected, we see that the thicker double-sided material is stronger than the thinner one overall, though the thinner, single-sided fabric performs the best. We hypothesize that this occurs because of errors introduced by slipping; the TPU is more slick than the ripstop material, and therefore may introduce additional uncertainty in the double-sided tests.

For the seam trials, we see an overall decrease in performance from the material trials, though ultimate tensile strength remains suitably high. In single-sided trial A, our collected data were noisy, preventing us from using a linear fit. Additionally, when conducting our double-sided thin trials, the TPU began to shear off the material, providing unusable results. That said, we still note that we see a 22% decrease in performance between material and seam tests for the single-sided trial and a 3% decrease for the double-sided thick trial, which gives us confidence that the reduction in seam strength for the double-sided thin trial would yield a similarly acceptable decrease.

Due to material and testing apparatus constraints, we were unable to conduct double-sided thin temperature tests. In addition, we had Instron calibration issues that retroactively made our single-sided trials unusable. Considering just the double-sided thick trials, we see an increase in performance over the room-temperature material trials, which was surprising to us given the apparent brittle failure of the fabric. We attribute this to the fact that our dogbones were so much shorter, which reduces the probability of encountering a severe flaw within the gauge length of the sample during testing. As a result, the material tended to fail later, giving us non-representative data that overstated material strength.

Finally, we note a small but significant increase in strain (and thus deformation) in our cyclic trials. After 20 cycles, the double-sided thick fabric experienced the most dramatic increase in strain, indicating that while it may be the strongest, it is also the most susceptible to cycling. In all three materials, the difference in strain between the first and last cycle is about 5% of the total strain. This indicates that there is a notable decrease in performance over time, but that the materials are still robust enough for our airbag application (especially given the high loads applied during testing).

IV. CONCLUSION

The Khione Bag offers a novel, accessible alternative to existing market-available avalanche airbags. In this paper, we have explored design performance as it relates to avalanche airbag standard EN 16716, focusing particularly on our dual-walled inflation scheme and the durability of our materials.

Through the use of multiple one-dimensional differential equation models, we showed that the novel dual-walled inflation scheme should function as intended, and were able to optimize the airbag's internal nozzle for maximum performance. We also demonstrated the scheme on a simplified, scaled-down physical prototype. In addition, through a series of tensile tests, we proved that our materials and manufacturing methods are more than strong enough to withstand airbag inflation forces. We also explored repeated deployments and temperature cycling, demonstrating minimal decrease in performance for multiple inflation but leaving open questions about airbag performance in the cold.

REFERENCES

[1] "Disasters explained: Avalanches." https://shelterbox.org/disasters-explained/avalanches/#:~:text=How%20many%20deaths%20do%20avalanches,increases%20their%20frequency%20and%20intensity, 03 2021.

[2] A. Avitt, "When snow becomes deadly: How to survive an avalanche." https://www.usda.gov/about-usda/news/blog/when-snow-becomes-deadly-how-survive-avalanche#:~:text=Every%20year%20roughly%20100%2C000%20avalanches%20sweep%20down,the%20U.S%20while%20skiing%2C%20snowboarding%2C%20and%20snowmobiling., 02 2021.

[3] H. Brugger, B. Durrer, F. Elsensohn, P. Paal, G. Strapazzon, E. Winterberger, K. Zafren, and J. Boyd, "Resuscitation of avalanche victims: Evidence-based guidelines of the international commission for mountain emergency medicine (icar medcom)," *Resuscitation*, vol. 84, p. 539–546, May 2013.

[4] S. E. McIntosh, C. E. Little, T. D. Seibert, N. E. Polukoff, and C. K. Grissom, "Avalanche airbag post-burial active deflation — the ability to create an air pocket to delay asphyxiation and prolong survival," *Resuscitation*, vol. 146, p. 155–160, Jan 2020.

[5] F. Hellberg, "The standard en 16716 for avalanche airbag systems." https://edelrid.com/us-en/knowledge/knowledge-base/abs-standard-avalanche-airbag-systems, 2024. Accessed: 2025-05-12.

[6] H. Struchtrup, *Thermodynamics and Energy Conversion*. Springer, 08 2014.

[7] T. Benson, "Mass flow rate equations," n.d. NASA Glenn Research Center. [Online]. Available: https://www.grc.nasa.gov/www/k-12/VirtualAero/BottleRocket/airplane/mchkdrv.html.

[8] J. Mitchell, R. Fox, and A. McDonald, *Fox and McDonald's Introduction to Fluid Mechanics*. John Wiley & Sons, Limited, 2020.

[9] E. Houghton, P. Carpenter, S. H. Collicott, and D. T. Valentine, "Chapter 1 - basic concepts and definitions," in *Aerodynamics for Engineering Students (Sixth Edition)* (E. Houghton, P. Carpenter, S. H. Collicott, and D. T. Valentine, eds.), pp. 1–68, Boston: Butterworth-Heinemann, sixth edition ed., 2013.

[10] F. Pinto, "System retrofit upgrades brochure." https://www.instron.com/wp-content/uploads/2024/06/System-Retrofit-Upgrades-Brochure.pdf, 2024. Accessed: 2025-05-12.

V. APPENDIX

A. Constants and Initial Values

Constant	Value	Unit
p_{amb}	1.05×10^5	Pa
T_{amb}	273	°K
A_1	3.77×10^{-7}	m^2
V_1	4.26×10^{-4} (26)	m^3 (in^3)
V_2	2.40×10^{-2} (24)	m^3 (L)
V_3	9.60×10^{-2} (96)	m^3 (L)
γ	1.4	–
R	297.05	$\frac{J}{kg \cdot K}$
C_d	0.6	–

TABLE IV
CONSTANTS USED IN THE COMPUTATIONAL MODELS

Variable	Initial Value	Unit
p_1	2.07×10^7	Pa
p_2	p_{amb}	Pa
p_3	p_{amb}	Pa
T_1	T_{amb}	°K
T_2	T_{amb}	°K
T_3	T_{amb}	°K

TABLE V
INITIAL VALUES FOR EACH CHAMBER OF THE COMPUTATION MODELS

B. Derivation of Uncertainty Propagation: Tensile Analysis

Uncertainty arose at many points during our tensile testing procedure and analysis, which we attempt to quantify here. Referring back to Eq. 6 for stress and strain, we see that there are five relevant measured quantities: the material thickness and width, t and w, which are needed to calculate the cross-sectional area A, the measured force and displacement values, F and l, and the initial length of the sample, l_0.

Because we stenciled and cut each of our dogbone samples ourselves, there is uncertainty error in the width and length values. We estimate this to be ± 1 mm in each dimension for any given sample based on the precision of our scissors and template:

$$\sigma_w = 1; \quad \sigma_{l_0} = 1$$

Propagating this forward, the uncertainty on the cross-sectional area ($A = w\bar{t}$) of each sample is given as such:

$$\sigma_A = \sqrt{A^2 \left[\left(\frac{\sigma_w}{w} \right)^2 + \left(\frac{\sigma_{\bar{t}}}{\bar{t}} \right)^2 \right]} \tag{7}$$

There is also uncertainty error in the thickness measurement of each sample, which was determined using a pair of calipers. Each thickness value used to calculate stress and strain is actually the average of three attempts, meaning we report $\bar{t}$ with an uncertainty equal to the standard error of the mean of the three trials:

$$\sigma_{\bar{t}} = \sqrt{\frac{\sum_{i=1}^{N} (t_i - \bar{t})^2}{N}} \tag{8}$$

We also have to consider the uncertainty of the data collected by the Instron. Using the data sheet for our machine, we determined that the load cell reports values accurate to 0.5% of the force measurement, and that the displacement values are accurate to 0.01 mm or 0.05% of the displacement, whichever is greater [10]. Aside from this bias error, there is also notable uncertainty error on the load cell due to drift. While we zeroed the force measurements before every trial, we estimate an additional ± 2 N uncertainty to compensate for this:

$$\sigma_F = \frac{0.5}{100} F + 2; \quad \sigma_l = max \left(0.01, \frac{0.05}{100} l \right)$$

From here, using Eq. 6 as a reference, we can compute the ultimate strength uncertainty σ_{σ_u} like:

$$\sigma_{\sigma_u} = \sqrt{\sigma_u^2 \left[\left(\frac{\sigma_F}{F} \right)^2 + \left(\frac{\sigma_A}{A} \right)^2 \right]} \tag{9}$$

In the end, we compute an average $\bar{\sigma_u}$ for each trial. Therefore, we report the standard error of the mean as the uncertainty on each $\bar{\sigma_u}$ value:

$$\sigma_{\bar{\sigma_u}} = \sqrt{\frac{\sum_{i=1}^{N} (\sigma_{u,i} - \bar{\sigma_u})^2}{N}} \tag{10}$$

For strain, we first compute the error of the difference ($\Delta l = l - l_0$). (We also note that this method applies to computing the difference in strains themselves for the cyclic comparison.)

$$\sigma_{\Delta l} = \sqrt{\sigma_l^2 + \sigma_{l_0}^2} \tag{11}$$

And finally, the strain itself referencing Eq. 6:

$$\sigma_\epsilon = \sqrt{\epsilon^2 \left[\left(\frac{\sigma_{\Delta l}}{\Delta l} \right)^2 + \left(\frac{\sigma_{l_0}}{l_0} \right)^2 \right]} \tag{12}$$